# 1. Investigations for High Prandtl Fluid

## 1.1 Study of Oscillatory Thermocapillary Flow of High Prandtl Number Fluid

*Yasuhiro Kamotani*

*Case Western Reserve University*

# STUDY OF OSCILLATORY THERMOCAPILLARY FLOW OF HIGH PRANDTL NUMBER FLUID

**Y. Kamotani[1], L. Wang[1], S. Hatta[1], P. Bhunia[1], and S. Yoda[2]**

[1]Case Western Reserve University, Cleveland, Ohio 44106, USA
[2]National Space Development Agency of Japan, 2-1-1 Sengen, Tsukuba, 305-8505, Japan

The effect of surrounding air motion on oscillatory thermocapillary flows is studied experimentally. Thermocapillary flows in liquid bridges and circular containers are investigated. The air motion is due to the natural convection of air caused by the heating-cooling arrangement of the experiment and also due to the forced convection associated with the motion of the liquid free surface. The air motion is varied in the present experiment by changing the cold wall temperature relative to the ambient air temperature. It is shown that in certain configurations the hot wall temperature at the onset of oscillations remains nearly unchanged when the cold wall temperature is varied over a wide range, which results in a substantial change in the critical Marangoni number ($Ma_{cr}$). In order to understand this unusual effect in detail, the air motion is simulated numerically, which shows a relatively weak air motion along the liquid free surface. It is shown that the overall air motion is dominated by natural convection in the liquid bridge configuration and by forced convection in the circular container configuration. The relation between $Ma_{cr}$ and the free surface heat loss caused by the air motion is discussed.

## 1. INTRODUCTION

Much work has been done on oscillatory thermocapillary flows, both theoretically and experimentally. However, the cause of oscillatory flow for high Prandtl number (Pr) fluid is not yet fully understood. The most widely investigated configuration is the half-zone (or liquid-bridge) configuration, in which a liquid column is suspended between two differentially heated walls. Much experimental information is available concerning the condition for the onset of oscillations in this configuration with high Prandtl number fluids (e.g. Preisser et al. [1]). These data have been taken by many investigators under various conditions with various experimental procedures. One reason for the lack of full understanding of the oscillation phenomenon is that those data are not very consistent. There are several causes for the discrepancy, as discussed by Masud et al. [2], but two main effects are those of buoyancy and liquid column shape. Not much attention has been given to the effect of heat transfer from the free surface. The effect of heat loss on the onset of oscillations has been investigated in the linear stability analysis by Kuhlmann and Rath [3], which shows that the heat loss must be appreciable for it to have an important effect for high Pr fluid. For many room temperature experiments, the Biot number associated with the surrounding airflow is less than unity, so its effect on the basic flow is considered to be small. Since our microgravity experiments on oscillatory thermocapillary flows in cylindrical containers were conducted with the cold wall temperature much lower than in our ground-based tests [4,5], we investigated, after the flight, the effect of the cold wall temperature. Then, we discovered that the cold wall temperature has an appreciable effect on the onset of oscillations under

certain conditions. This motivated our recent investigation on the surrounding air motion effect on oscillatory thermocapillary flows.

Usually, thermocapillary flow tests with high Pr fluids (mainly silicone oils) are conducted in room air. Then, the heat transfer from the free surface is mainly caused by the motion of ambient air. In high temperature tests, radiation heat transfer at the free surface is also important, but we will only consider near room temperature tests herein. The air motion is caused by buoyancy due to a non-uniform temperature distribution in the air produced by the heating and cooling done in the test. The liquid free surface motion also induces air motion, which is important in microgravity. The heat loss (or gain) due to the air motion can be controlled by adjusting the overall fluid temperature level relative to the ambient temperature. In the present experiments the conditions for the onset of oscillations are investigated under variable free surface heat transfer. Both half-zone and circular cylinder configurations are investigated. It is shown that the free surface heat transfer effect is significant.

In conjunction with the experiments, the air motion is also simulated numerically to determine its magnitude and extent and to compute the heat transfer rate from the liquid free surface.

## 2. CONFIGURATIONS AND IMPORTANT PARAMETERS

The half-zone configuration is illustrated in Fig. 1. The top and bottom walls are maintained at constant but different temperatures. We have conducted the Surface Tension Driven Convection Experiment (STDCE) in microgravity in cylindrical containers [4,5]. The STDCE configurations are illustrated in Fig. 2. Two heating methods were employed: heating by a cylindrical heater placed along the container centerline (called the CT configuration, see Fig. 2(a)) and external heating by a $CO_2$ laser beam (called the CF configuration, Fig. 2(b)). We have observed oscillatory flows in all of these configurations.

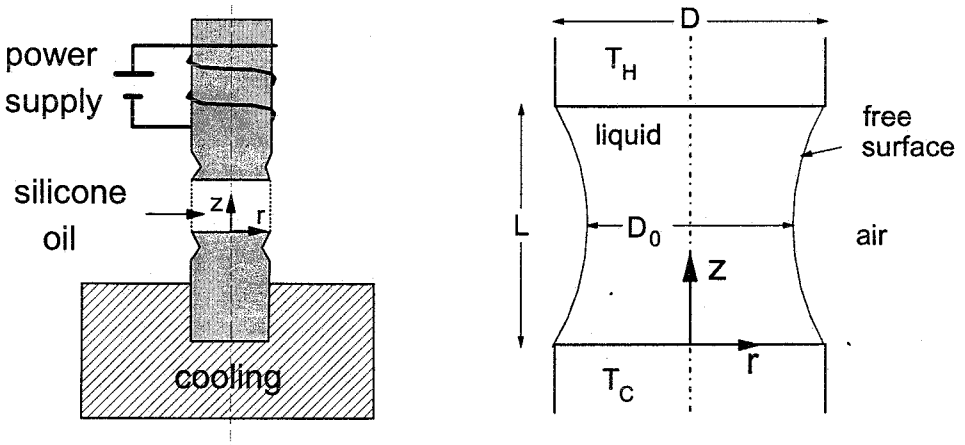


Fig. 1 Half-zone configuration

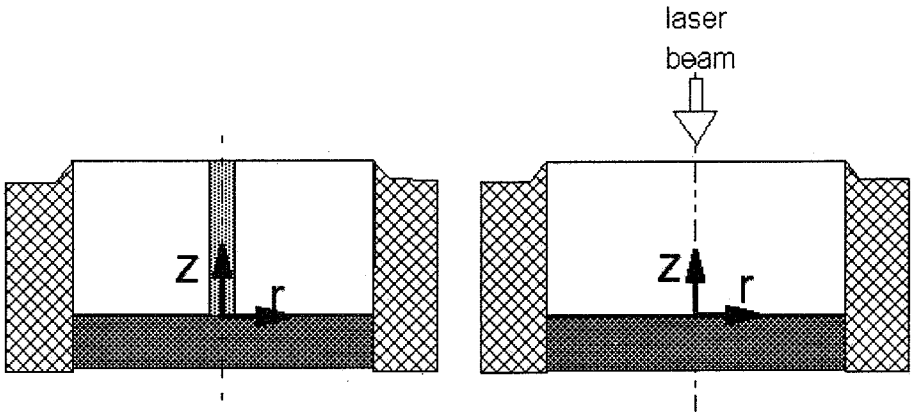


(a) CT Test Container (b) CF Test Container

Fig.2 STDCE configurations

The important dimensionless parameters for the thermocapillary flows in these configurations are known to be: Marangoni number $Ma = \sigma_T \Delta T_L L_1/\mu\alpha$, Prandtl number $Pr = \nu/\alpha$, and aspect ratio $Ar = L_1/L_2$, where $\sigma_T$ is the temperature coefficient of surface tension, $\Delta T_L$ is the overall temperature variation in the liquid, $\mu$ is the dynamic viscosity of the liquid, $\nu$ is the liquid kinematic viscosity, and $\alpha$ is the liquid thermal diffusivity. $L_1$ is the liquid column length in the half-zone configuration and the container radius in the STDCE configurations. $L_2$ is the liquid column diameter in the half-zone configuration and the container depth in the STDCE configurations. In the present work, we minimize the effects of buoyancy and gravity by using small dimensions. It is known that the oscillation phenomenon in the half-zone configuration is sensitive to the free surface shape. Therefore, in some tests we reduce the amount of liquid so as to make the free surface concave. The concave shape is represented by Dr, which is the ratio of the liquid column diameter near the mid-height (see Fig. 1) to that at the base. According to our past work, the condition for the onset of oscillations for high Pr fluid in the liquid bridge configuration is specified by two parameters: Ma and a surface deformation parameter [6]. Both parameters must become large enough for the transition to occur. One parameter is more important than the other depending on the size of the liquid column. In the parametric range of the present experiment, Ma controls the transition, so the critical Marangoni number ($Ma_{cr}$) is used for all the configurations investigated herein. A parameter representing the surface heat transfer will be defined later.

## 3. EXPERIMENTS

The experimental apparatus for the liquid bridge configuration is similar to the one used in our past experiments (e.g. [2]). The top and bottom walls are made of copper rods. The top rod is heated by a nichrome wire coiled around it. The bottom rod is connected to a large copper block that is cooled by circulating water from a constant temperature bath. The temperatures of the top and bottom copper rods are measured by imbedded thermocouples. The test fluids are 2- and 5-centistokes (cSt) silicone oils. In order to minimize buoyancy, we use 2- and 3-mm diameter liquid columns in the present experiments. Ar is kept nearly constant, Ar = 0.65 - 0.70. The length of the top copper rod is 12 mm. The bottom rod length is 9 mm and is connected to the cylindrical copper block of diameter 24 mm. Usually

in the liquid bridge configuration, the top rod is heated, but we test both the heated-from-above and the heated-from-below configurations in the present work. In order to vary the ambient air temperature, the apparatus is placed in an oven in some tests. The oven has the interior dimensions of 28 cm (width) x 25 cm (height) x 25 cm (depth). Hot air is circulated within the oven by natural convection (a gravity convection oven). The circulating air motion is observed to be much weaker than the local air motion around the liquid column due to the hot and cold rods. The parametric ranges covered by the present experiments in the liquid bridge configuration are: $Ma < 3.5x10^4$, $20 < Pr < 55$, Ar=0.65-0.7, and $0.6 \leq Dr \leq 1$. For Ma and Pr, the fluid properties are evaluated at the fluid mean temperature, $\frac{1}{2}(T_H + T_C)$.

In the STDCE experiments in microgravity we found that the conditions for the onset of oscillations were nearly the same in normal gravity and in microgravity for the container diameter less than or equal to 1.2 cm. Since the flight hardware for STDCE is still operational, we use it with the 1.2 cm diameter container. The experiment is described in [4,5] and the STDCE hardware is described in [7]. The parametric ranges covered in the STDCE configurations are: $Ma < 2.5x10^4$, $20 < Pr < 25$, and Ar=1.0. Only flat free surface tests are conducted.

The onset of oscillations is identified by flow visualization in liquid bridges and from the IR images of the free surface in the STDCE configurations.

## 4. NUMERICAL SIMULATIONS OF AIR MOTION

Since it is difficult to investigate the air motion in detail and to determine the heat transfer rate at the liquid free surface experimentally, the motion is simulated numerically. The simulation is done only for a flat free surface. The airflow and the liquid flow are solved simultaneously. The simulations are done only for steady flows.

The flow in the liquid is assumed to be steady and axisymmetric. We have developed a numerical code based on SIMPLER [8] to analyze steady thermocapillary flows and its predictions have been extensively tested (e.g. [9,10]). We use the same program herein. A non-uniform grid is employed with meshes graded toward the hot and cold walls and toward the free surface.

The same program is modified to analyze the airflow. The airflow is assumed to be laminar and axisymmetric. The Boussinesq approximation is employed. The Prandtl number of the air is set equal to 0.7. The computational domains for the airflow analysis are defined in Fig. 3. In the half-zone configuration, the cold wall, including the copper block, is maintained at $T_C$. The diameter of the cold copper block (1.2 cm=$R_C$) defines the diameter of the outer computational boundary. In the STDCE/CT configuration, the computational domain is 2.4 cm in radius (=$R_C$) and 1.5 cm in height (=H). Along the open boundaries, the airflow comes in or goes out. In the region where the flow comes in, the temperature is set equal to the ambient temperature, and in the region where it goes out, the temperature gradient is set to be zero normal to the boundary. Both velocity components are assumed to have zero normal gradients along the open boundaries.

At the free surface, the velocity, temperature, and heat flux are continuous. The viscosity ratio of air to silicone oil is roughly 0.005, while the thermal conductivity ratio is much larger (about 0.23). Therefore, the effect of shear due to the air motion on the

thermocapillarity condition is neglected. In addition to the heat loss due to convection, the loss due to radiation is included. The emissivity of the test fluids is known to be 0.9. It is found that the radiation contribution to the total heat loss is less than 15%.

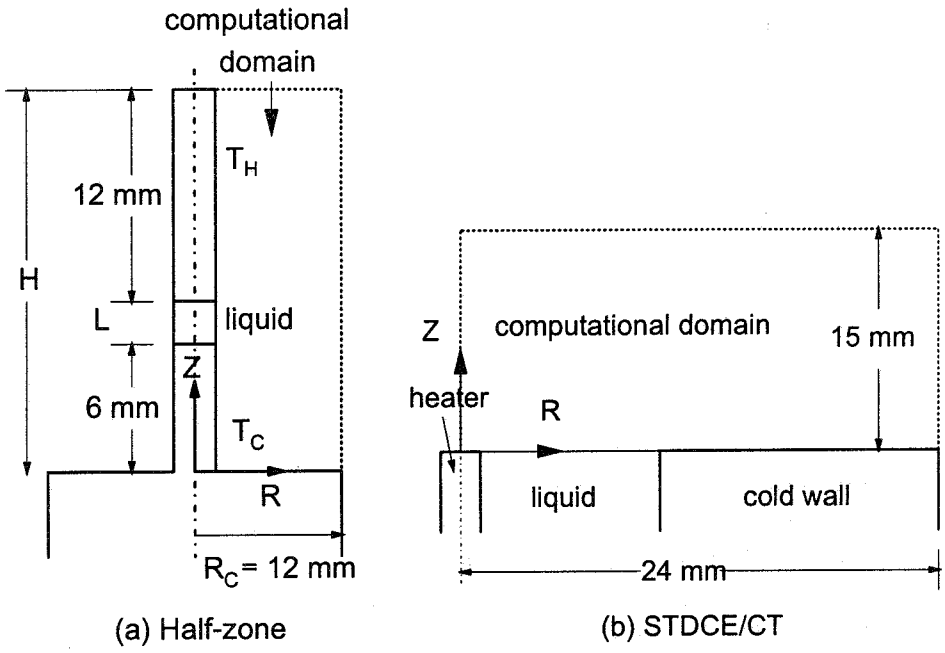


Fig.3 Computational domains for airflow analysis

## 5. RESULTS AND DISCUSSIONS

### 5.1. Effect of free surface heat transfer on onset of oscillations

In a typical test, we fix $T_C$ at a desired value and then gradually increase $T_H$ until the flow becomes oscillatory. The temperature difference $\Delta T_L$ at the transition is called the critical temperature difference, $\Delta T_{cr}$. $\Delta T_{cr}$ is non-dimensionalized as $Ma_{cr}$. Tests are conducted with various values of $T_C$. Room temperature is constant during these tests.

#### 5.1.1. Results for liquid bridge configuration

The effects of $T_C$ on $\Delta T_{cr}$ under various conditions are presented in Figs. 4-7 for the half-zone configuration. Both dimensional and dimensionless onset conditions are shown for each case. Two distinct trends are found when Dr is varied. When the free surface is concave (Dr $\leq$ 0.8), as $T_C$ is increased, $T_H$ at the onset of oscillations increases in such a way that $\Delta T_{cr}$ remains nearly constant (Figs. 4 and 5). $\Delta T_{cr}$ slightly decreases with increasing temperature level because of decreasing fluid viscosity. Therefore, if $\Delta T_{cr}$ is non-dimensionalized as $Ma_{cr}$, with the viscosity evaluated at the fluid mean temperature, $Ma_{cr}$ does not change with $T_C$ within the experimental error, as seen Figs. 4 and 5. The result is what one would expect when Ma is the main parameter.

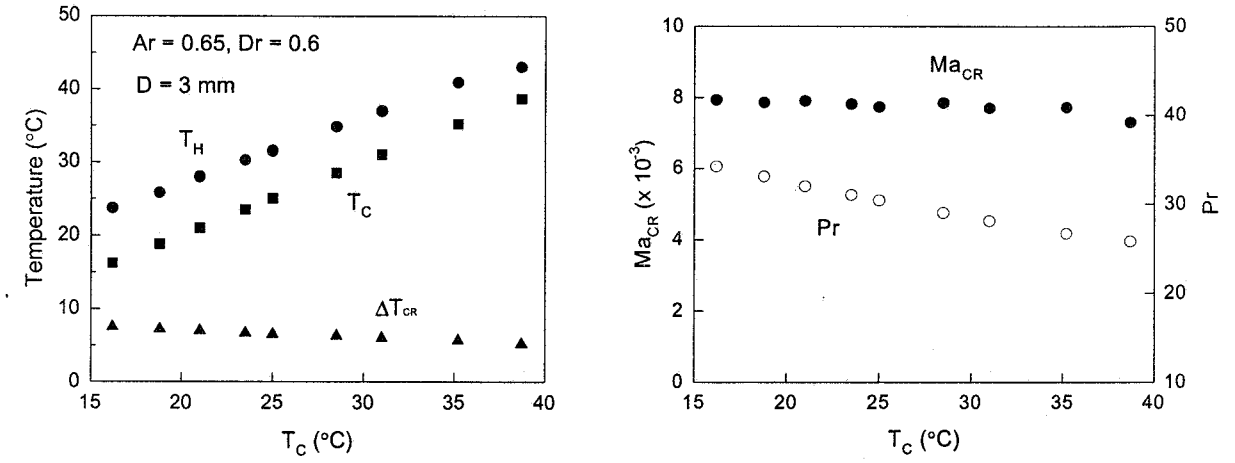


Fig. 4 Critical conditions in half-zone configuration for Dr=0.6

On the other hand, when the free surface is nearly flat ($0.9 \leq Dr \leq 1.0$), the trend is quite different. As Fig. 6 shows for Dr = 1, $T_H$ remains nearly constant even when $T_C$ is varied from 14 to about 30 °C, which means $\Delta T_{cr}$ decreases with increasing $T_C$. As seen in Fig. 6, the change of $Ma_{cr}$ is substantial: There is a 70% reduction in $Ma_{cr}$ when $T_C$ is varied from 14 to 35 °C. Although the fluid viscosity (and Pr) changes with $T_C$, as shown in Fig. 6, the variation of Pr is not large enough to explain such a large change in $Ma_{cr}$. This significant $T_C$ effect is the main subject of the present work. Beyond a $T_C$ of about 30 °C, $T_H$ increases with increasing $T_C$ in such a way that $Ma_{cr}$ remains nearly constant (around 7,000). The same trend can be seen for Dr = 0.9 (Fig. 7). It is noted that there is no gradual change from one trend to the other when we change Dr, we simply have one of the two trends for a given Dr.

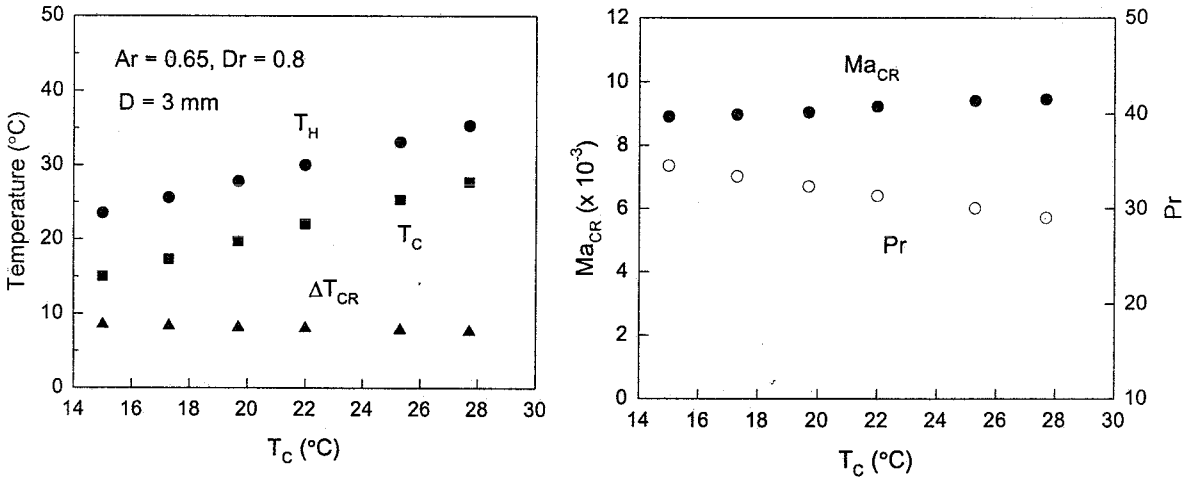


Fig. 5 Critical conditions in half-zone configuration for Dr=0.8

It is known that when Dr (or the free surface shape) is varied while keeping Ar constant, the $Ma_{cr}$-Dr curve has two branches, a fat branch (near flat surface) and a slender branch (concave surface) [2], as shown in Fig. 8. This is called the shape effect. For 2-cSt silicone oil and Ar = 0.7 the changeover occurs between Dr = 0.8 and 0.9. The two trends shown

above are found to correspond to those branches: $Ma_{cr}$ is not sensitive to $T_C$ in the slender branch, but it is very much affected by $T_C$ in the fat branch.

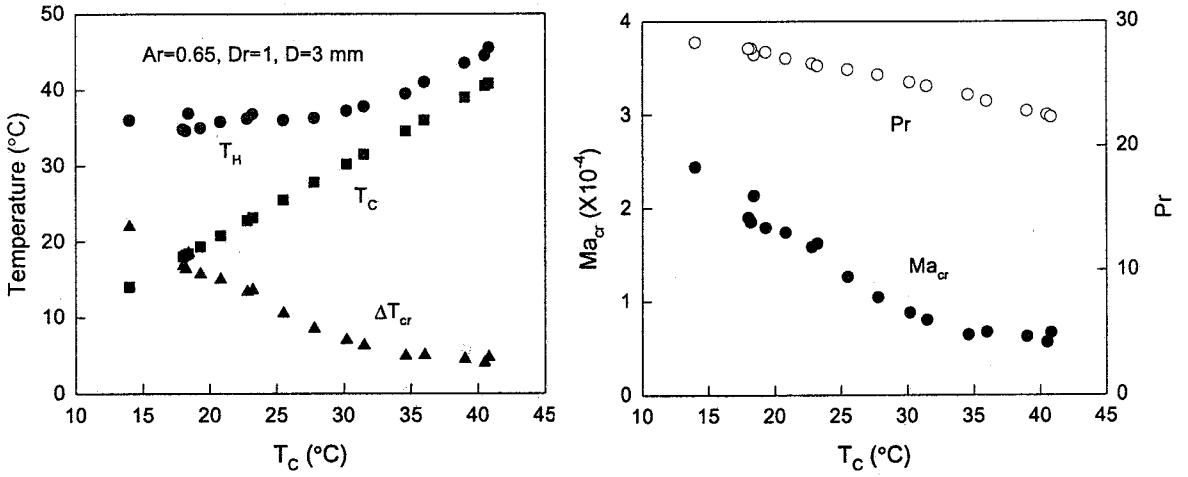


Fig. 6 Critical conditions in half-zone configuration for Dr=1.0

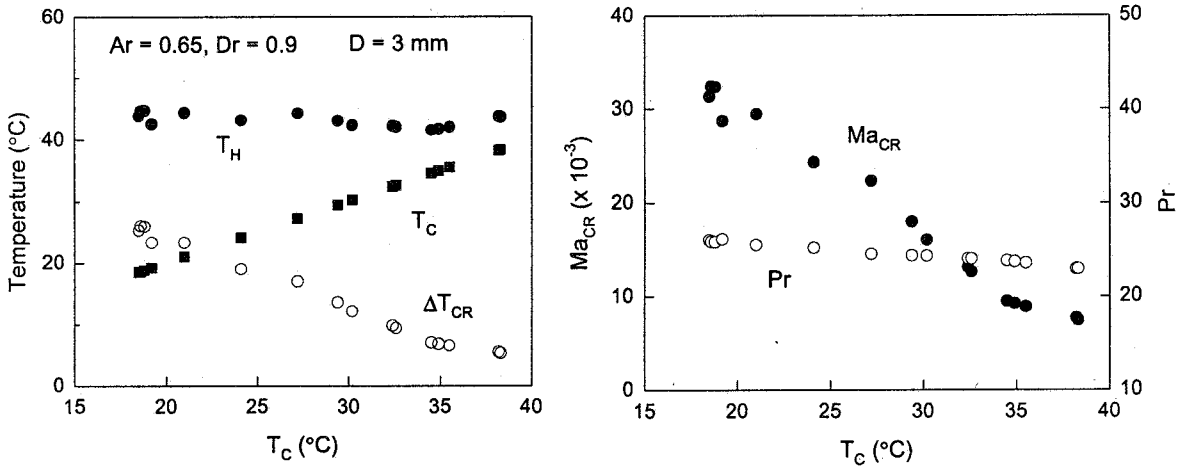


Fig. 7 Critical conditions in half-zone configuration for Dr=0.9

Before we go further, we discuss what this $T_C$ effect represents. By changing $T_C$ we are changing the motion of the surrounding air. One way to show this is to vary the surrounding air temperature, $T_R$. Since the air motion is due to forced and natural convection, the airflow does not change as long as $T_R - T_C$ is fixed, and thus $Ma_{cr}$ would remain unchanged if the airflow is responsible for the afore-mentioned variation in $Ma_{cr}$ with a nearly flat free surface. In order to see this, tests are conducted, most of them in the oven, while keeping $T_R - T_C$ nearly constant. The result presented in Fig. 9 shows that $Ma_{cr}$ is indeed unchanged within the experimental error when $T_C$ is varied. In another tests we conducted, in order to show that the effect of the airflow on the onset of oscillations, we placed an object near the liquid column (without touching it), which changes the airflow around the column. In Fig. 10 the result is shown from the test where an umbrella-like object made of a thin paper is placed around the heating rod just above the liquid. $Ma_{cr}$ is increased significantly with the umbrella.

It is thus clear that the onset of oscillations is affected by the airflow. As discussed earlier, the shear stress at the free surface caused by the airflow is negligibly small. Therefore, the airflow affects $Ma_{cr}$ only through the heat transfer at the free surface.

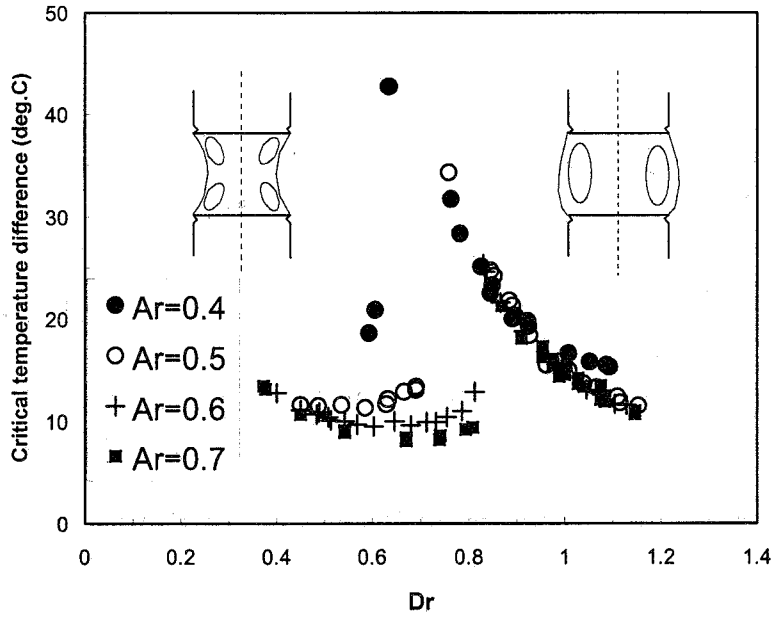


Fig. 8 Dependence of $Ma_{cr}$ on Dr in half-zone configuration

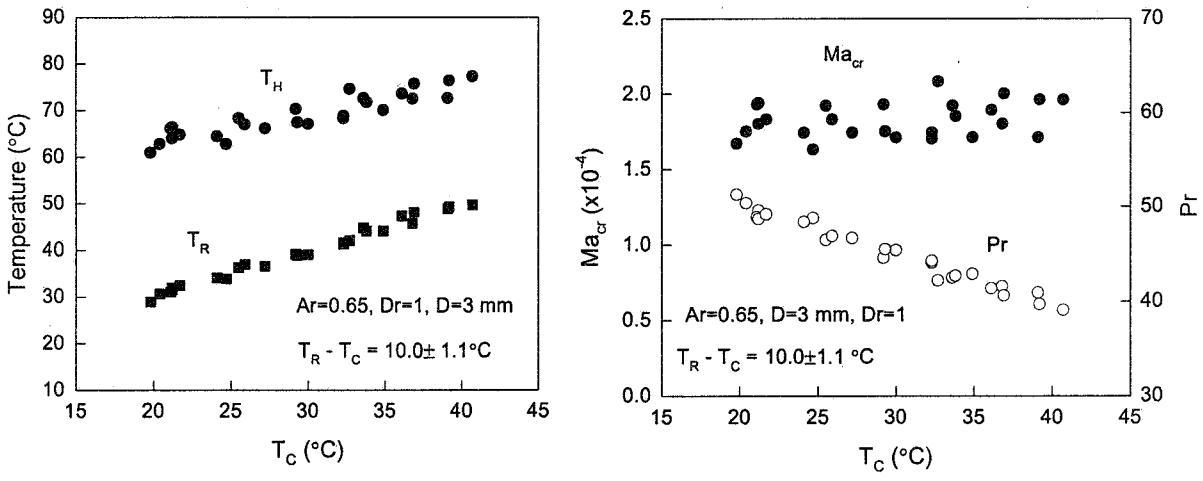


Fig. 9 Effect of $T_C$ on $Ma_{cr}$ while keeping air motion nearly fixed

Similar effect of $T_C$ can be seen when the liquid column is heated from below. One result is shown in Fig. 11. Although the data trend is similar to the one seen in the heated-from-above configuration, $Ma_{cr}$ is generally larger in the heated-from-below configuration for a given $T_C$. This difference in $Ma_{cr}$ can be attributed to the fact that the air natural convection is different in this configuration from that in the heated-from-above configuration.

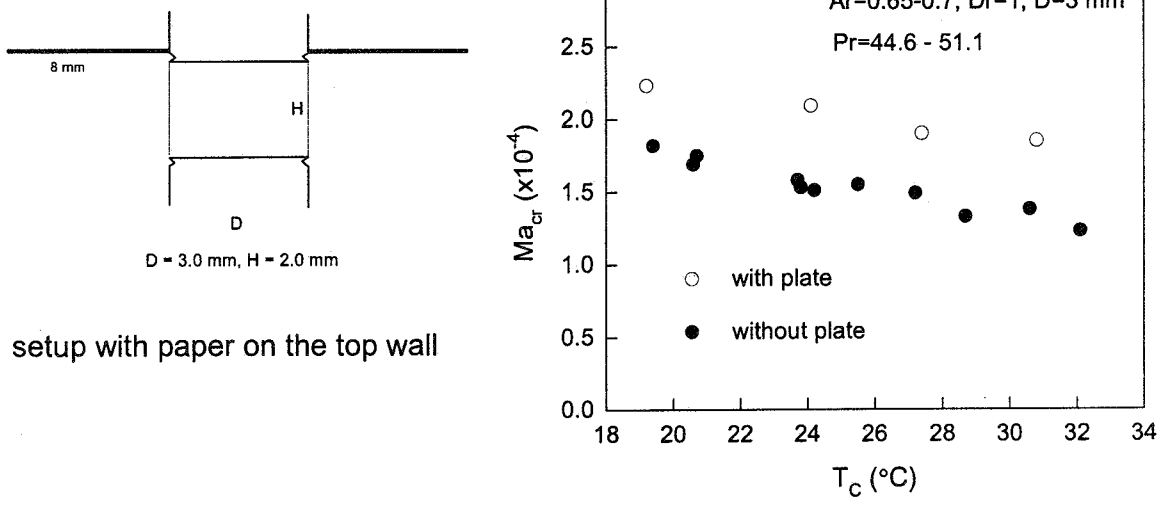


Fig. 10 Effect of top plate on $Ma_{cr}$

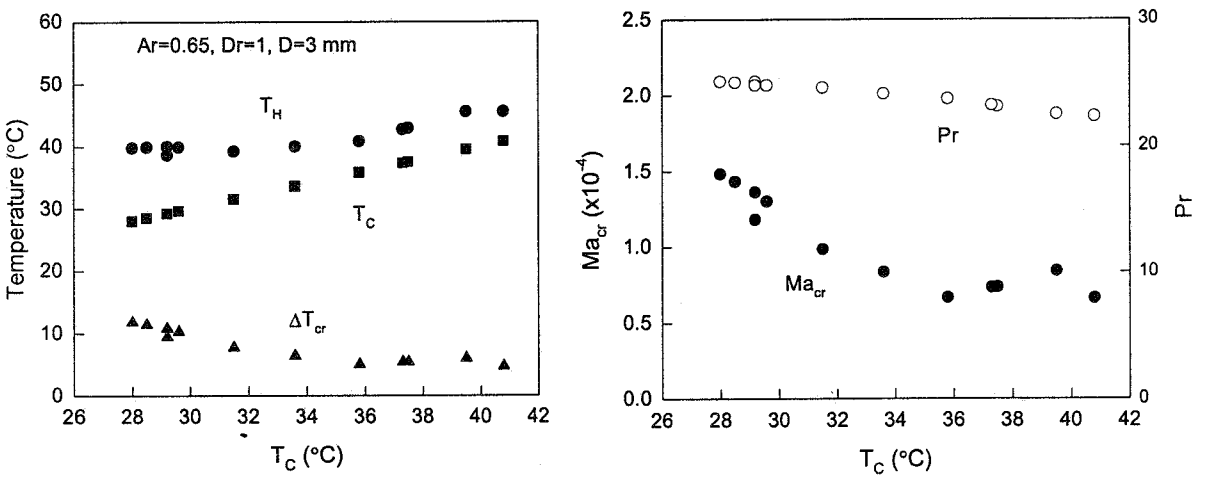


Fig. 11 Critical conditions in heated-from-below configuration for Dr=1.0

One unique feature of the airflow effect is that the value of $\Delta T_a = T_H - T_R$ at the onset of oscillations, for given fluid and liquid column dimensions, is nearly constant over a wide range of $T_C - T_R$. One typical trend is shown in Fig. 12. The figure shows that for a 50 °C variation of $T_C - T_R$, $\Delta T_a$ is relatively constant (31±2 °C), although $\Delta T_a$ increases slightly with increasing $T_C - T_R$. This trend is very interesting but it is not immediately obvious how this happens.

5.1.2. Results for STDCE configurations

The result for the STDCE/CT configuration is presented in Fig. 13. The only experimental variable in the tests is $T_C$. Hr in the figure is the ratio of the heater diameter to the container diameter (heater ratio). As seen Fig. 13, $T_H$-$T_R$ is nearly constant at the onset of oscillations, which is the same trend found in liquid bridges with nearly flat free surfaces. As a result, $Ma_{cr}$ decreases with increasing $T_C$ (Fig. 13). Again, the change in $Ma_{cr}$ is significant.

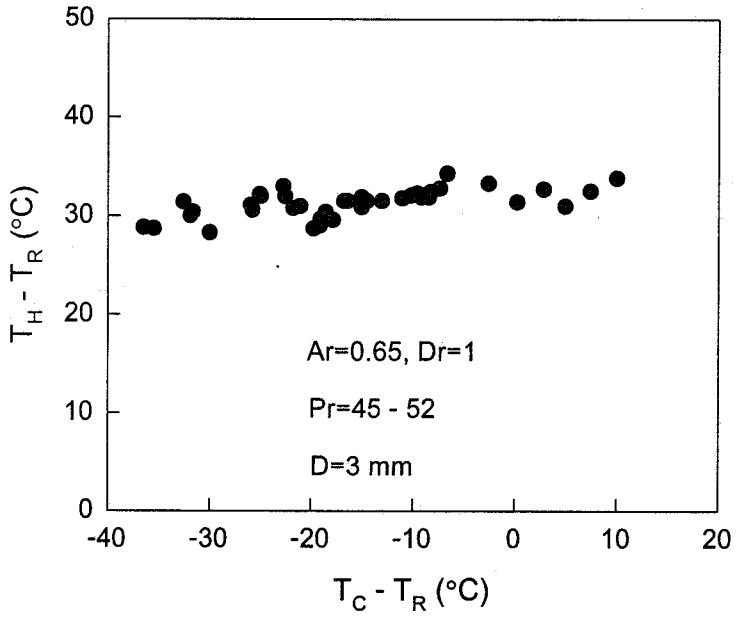


Fig. 12 $(T_H - T_R)$ versus $(T_C - T_R)$ at onset of oscillations

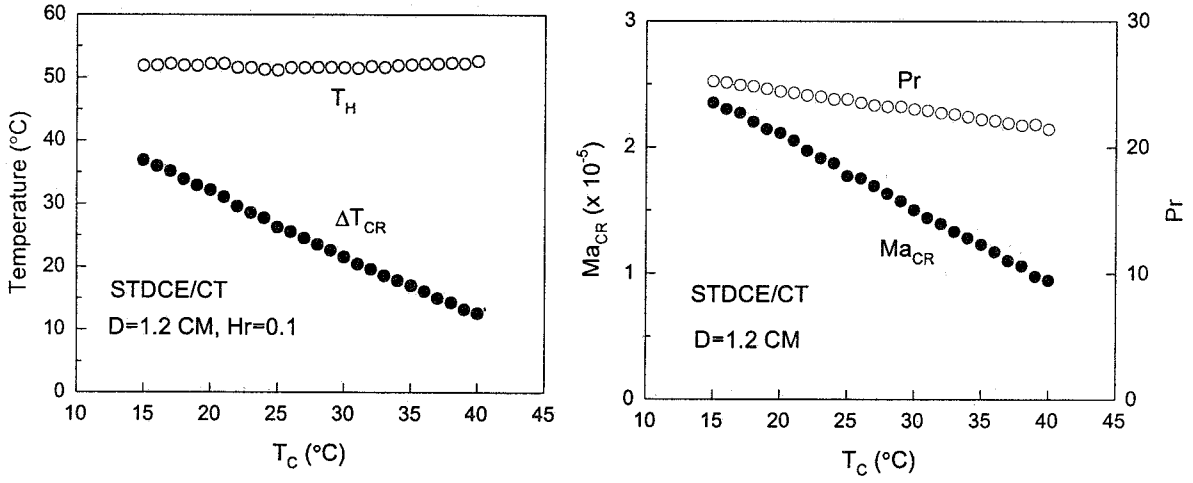


Fig.13 Critical conditions in STDCE/CT configuration

On the other hand, in the STDCE/CF configuration, $T_H$-$T_R$ varies at the onset of oscillations when $T_C$ is varied (Fig. 14). However, the variation of $Ma_{cr}$ with $T_C$ is much smaller than that in the CT configuration with the same Hr. Therefore, the trend in this configuration is closer to the trend found in slender liquid bridges.

In summary, the feature of our interest, namely strong sensitivity of $Ma_{cr}$ to $T_C$, is found in the liquid bridge configuration with nearly a flat free surface and in the STDCE/CT configuration.

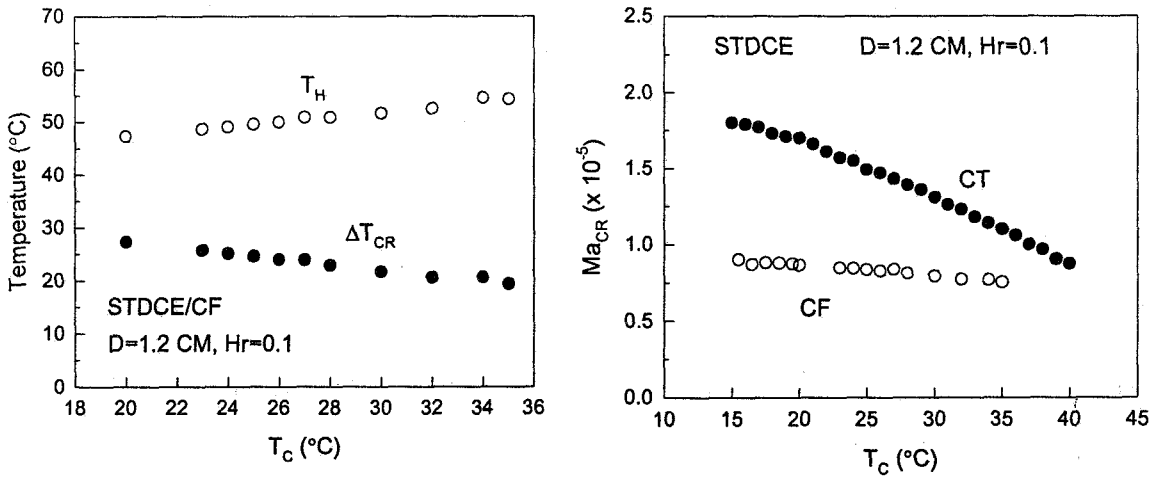


Fig.14 Critical conditions in STDCE/CF configuration

## 5.2. Numerical investigation of airflows

### 5.2.1. Airflow around liquid bridge

The above results show that it is important to study the airflow and the heat transfer at the liquid free surface. The computed streamline and isotherm patterns are shown to describe the airflow. They are shown only at the experimentally determined critical conditions.

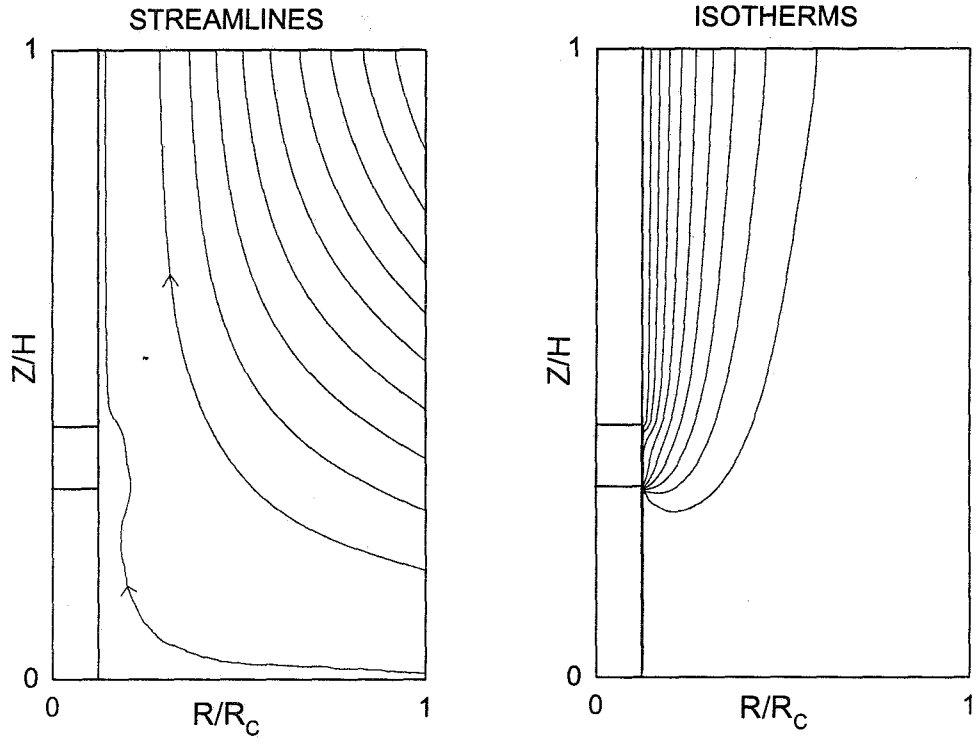


Fig. 15 Flow and temperature fields in half-zone configuration, heated-from-above ($Ma=1.6x10^4$, $Pr=27$, $Ar=0.65$, $T_C-T_R=0$ °C, $T_H-T_R=13.8$ °C)

The computed streamlines and isotherms are shown in Fig. 15 for a typical room temperature test in the half-zone configuration. The flow is mainly upward (note that $T_H$ is always larger than $T_R$ near the critical condition), except in the region near the liquid surface where a small recirculation cell appears as the flow caused by the surface shear is in the downward direction. The isotherms show a thermal boundary layer along the liquid surface and the hot wall. The boundary layer thickness is well within the outer computational boundary, which justifies the choice of its location. The airflow is driven by both the liquid shear and buoyancy. The present analysis shows that the liquid free surface velocity is nearly the same as the buoyancy driven flow velocity, both on the order of a few cm/s. However, the total air volume affected by this liquid motion is relatively small (note that this is a cylindrical configuration), as seen in Fig. 15. Consequently, the liquid shear effect on the heat transfer is relatively small. For example, for the conditions of Fig. 15, the heat loss increases by only 4.3% if we do not include the shear.

In the heated-from-below configuration, the buoyant flow and the shear-driven flow are in the same direction, so the airflow is upward everywhere in Fig. 16. The thermal boundary layer is thicker than that in Fig. 15 because of the hot horizontal bottom wall.

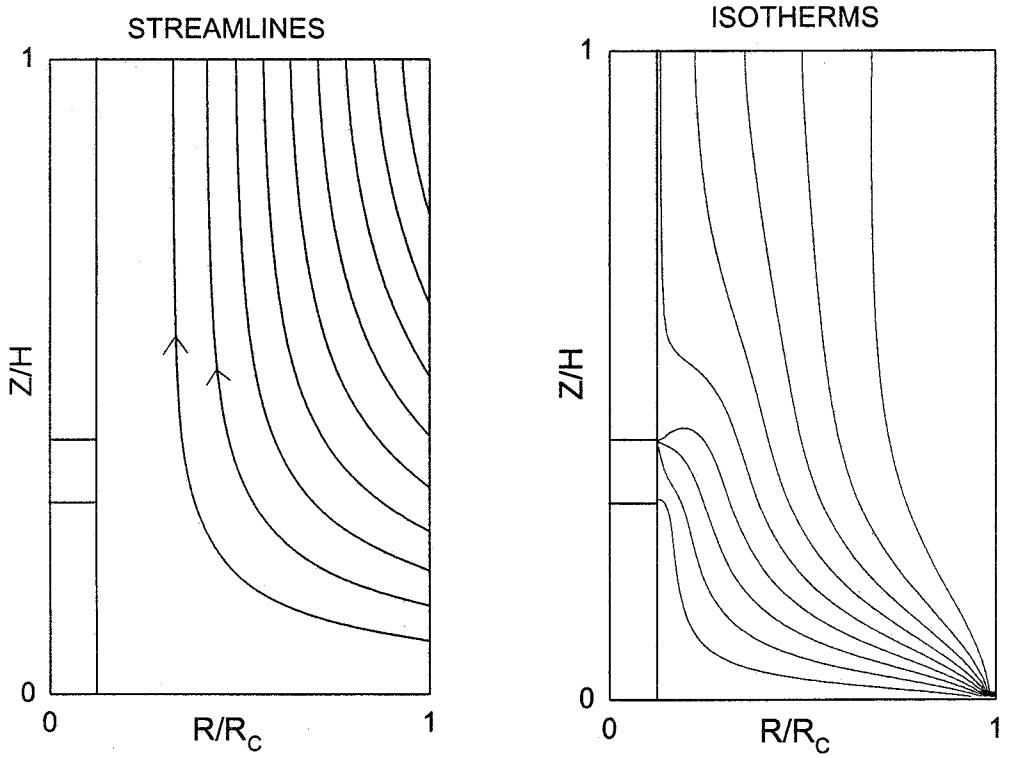


Fig. 16 Flow and temperature fields in half-zone configuration, heated-from-below ($Ma=7.3x10^3$, $Pr=23$, $Ar=0.65$, $T_C-T_R=5.6$ °C, $T_H-T_R=11.0$ °C)

In the oven tests, the surrounding air temperature is generally higher than $T_C$ but $T_H$ is always higher than the air temperature. Typical streamline and isotherm patterns are shown in Fig. 17. The airflow along the heater is upward, but it is downward along the cold wall. The stagnation point is located just above the liquid column. According to the isotherm pattern, the average liquid surface temperature is higher than the ambient temperature (the

isotherm in the middle in Fig. 17 is near the ambient temperature), so heat is lost from the free surface even in the oven tests.

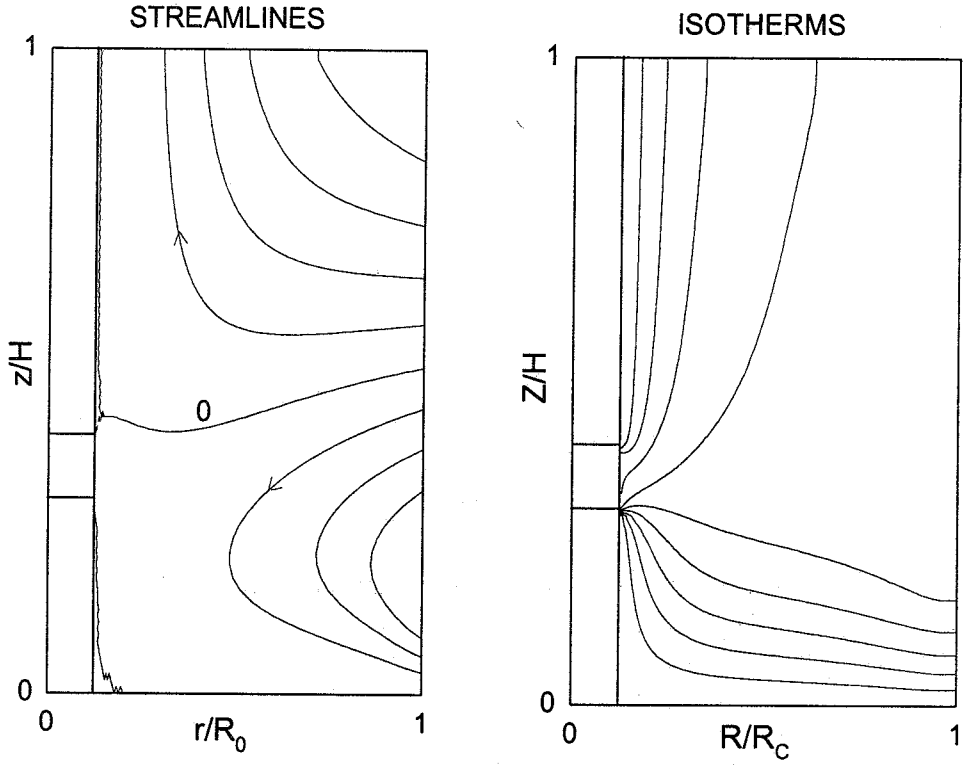


Fig. 17 Flow and temperature fields in half-zone configuration, heated-from-above in oven ($Ma=3.0x10^4$, $Pr=44$, $Ar=0.65$, $T_C-T_R=-37$ °C, $T_H-T_R=27$ °C)

5.2.2. Airflow in STDCE/CT configuration

The airflow structure in the STDCE/CT configuration is shown in Fig. 18. Unlike the liquid bridge configuration, there are no heated or cooled vertical surfaces in this configuration. Moreover, the hot wall is relatively small, so that the temperature variation in

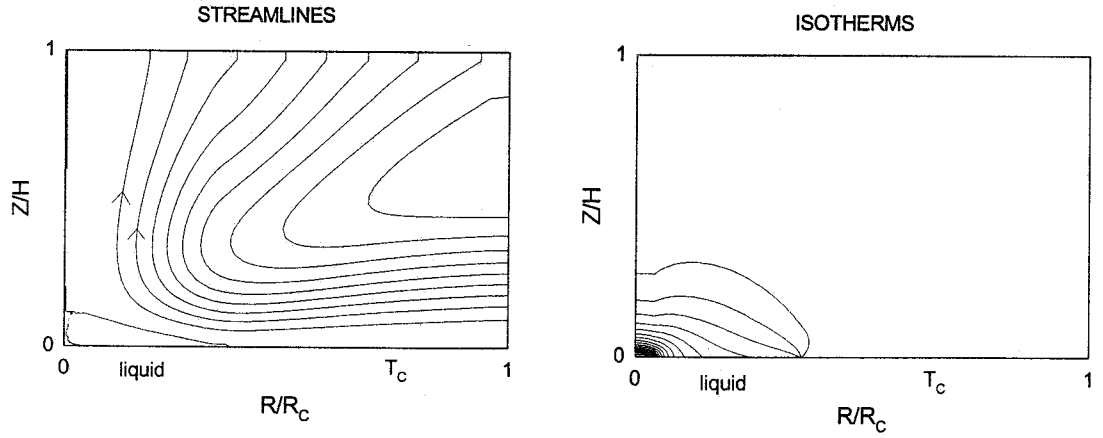


Fig. 18 Flow and temperature fields in STDCE/CT configuration ($Ma=1.1x10^5$, $Pr=24$, $Ar=1$, $T_C-T_R=0$ °C, $T_H-T_R=28.5$ °C)

the air occurs in a relatively small region in Fig. 18. Both factors result in weaker buoyancy-driven flow. As seen in Fig. 18, over most of the computational domain the flow field is dominated by buoyancy-driven flow with an upward motion above the liquid. Near the liquid surface, the flow is dominated by the shear-driven flow, resulting in a recirculating cell above the liquid (Fig. 18b).

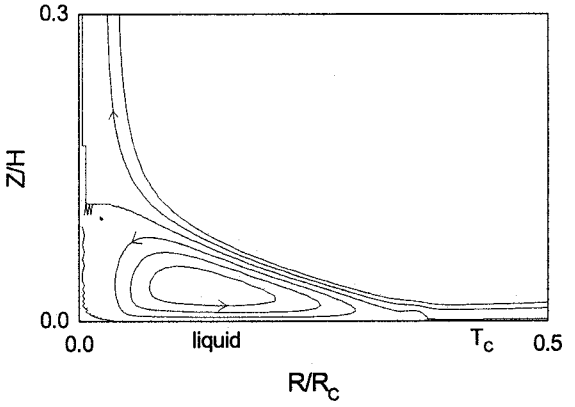


Fig. 18b Details of flow near free surface for Fig. 18

5.3. Relation between free surface heat transfer rate and $Ma_{cr}$

Since it is customary to relate the critical condition to a dimensionless parameter called the Biot number, we define the Biot number for the present configuration. We start with the liquid bridge configuration. The expression for the amount of heat loss per unit free surface area (q) is $k_L(\partial T_L/\partial r) = h\ (T_S - T_R) = q$. h is the heat transfer coefficient, $T_R$ is the air temperature, $T_S$ is the free surface temperature, and the subscript L is for the liquid phase. If we use the same reference temperature variation for both the liquid and gas phases, non-dimensionalization of this equation introduces the so-called Biot number ($hR/k_L$). However, in the present experiment, the temperature variation in the liquid and that in the air are independently controlled, so the Biot number does not properly represent the amount of heat loss. Therefore, we introduce a new parameter based on the heat flux instead of h. Locally we can define a parameter based on q, but in the present work we are mainly interested in the effect of overall heat transfer from the whole free surface. For that reason, we define a parameter based on the total heat loss from the free surface (Q). By integrating the equation $k_L(\partial T_L/\partial r) = q$ over the free surface, it can be shown that the average dimensionless temperature gradient at the free surface is represented by the parameter $Q/(2\pi L k_L \Delta T_L)$. We call this parameter a modified average Biot number (Bi*). Bi* takes into account the total heat loss from the free surface accurately. In the case of liquid bridge, the amount of conduction heat transfer through the liquid is $k_L(\Delta T_L/L)\pi D^2/4$ so that the ratio of the surface heat transfer rate to the conduction heat transfer rate can be expressed as $8Ar^2Bi^*$.

Similarly, in the CT configuration, it can be shown that the modified Biot number (or the average dimensionless surface temperature gradient) can be expressed as $Bi^*=QH/(\pi(R_C^2 - R_H^2)k_L\Delta T_L)$, where $R_H$ is the heater radius and $R_C$ is the container radius. The ratio of the surface heat transfer rate to the conduction heat transfer rate can be expressed as $(1-Hr^2)$ x $\log(1/Hr)/(2Ar^2)Bi^*$.

Therefore, for a given Ar (and Hr in the CT configuration), Bi* represents the ratio of those two heat transfer rates, or Bi* is a measure of how much the basic temperature field is distorted by the free surface heat transfer.

The critical conditions ($Ma_{cr}$) obtained in all of the present tests are now correlated by Bi*. We start with the half-zone configuration. As seen in Fig. 19, considering the fact that the figure is a combination of experimental and numerical results, Bi* seems to correlate the $Ma_{cr}$ data reasonably well for all the cases investigated herein. The two fluids used in the tests have different Pr values, but the effect of Pr cannot be detected in Fig. 19. In all cases Bi* is positive, meaning that heat is lost from the free surface on the average. The general trend of the data is that $Ma_{cr}$ decreases with increasing Bi*. When $Ma_{cr}$ is reduced to around 6,000, it does not change with further increase in Bi*. $Ma_{cr}$ attains a peak value when Bi* is below about 0.25. Between those two limits, $Ma_{cr}$ changes by a factor of about 5, but if we neglect the heat loss effect (as we have done in the past), all those tests are considered to be conducted under nearly the same conditions.

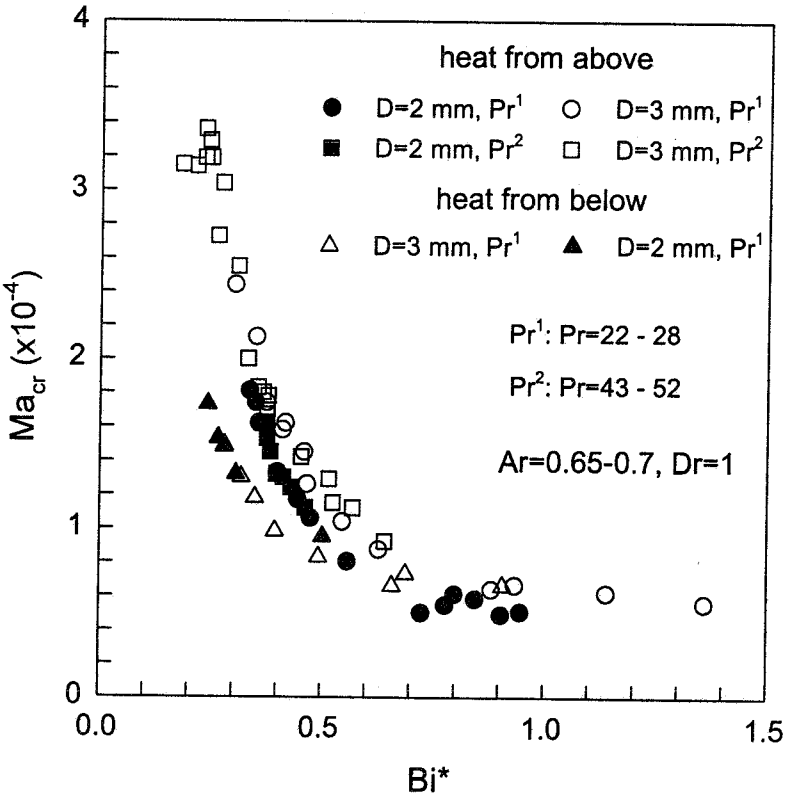


Fig. 19 $Ma_{cr}$ versus Bi* in half-zone configuration

The result for the CT configuration is shown in Fig. 20. As in Fig. 19, $Ma_{cr}$ decreases with increasing Bi*.

## 5.4. Discussion of heat loss effect

There are several important features of Figs. 19 and 20 that need to be discussed. (i) The onset of oscillations is affected by the heat loss even when Bi* is relatively small (the

heat loss effect is observed when Bi* is less than unity). For the STDCE/CT configuration, Bi* ranges from 0.1 to 0.8. In order to show how much the basic flow field is distorted by the heat loss, we present in Fig. 21 the computed surface temperature and velocity distributions with and without the heat loss for Bi*= 0.23 for the CT configuration. As seen in the figure, the distortion is quite small, yet the onset of oscillations is affected by the heat loss significantly even when Bi* is smaller. (ii) In the half-zone configuration, a large change in $Ma_{cr}$ occurs in a relatively small range of Bi*: $Ma_{cr}$ changes by a factor of about two when Bi* is varied from 0.25 to 0.35. Again, the change in the basic flow field is quite small when Bi* is varied from 0.25 to 0.35. (iii) We have to explain why $T_H - T_R$ is constant

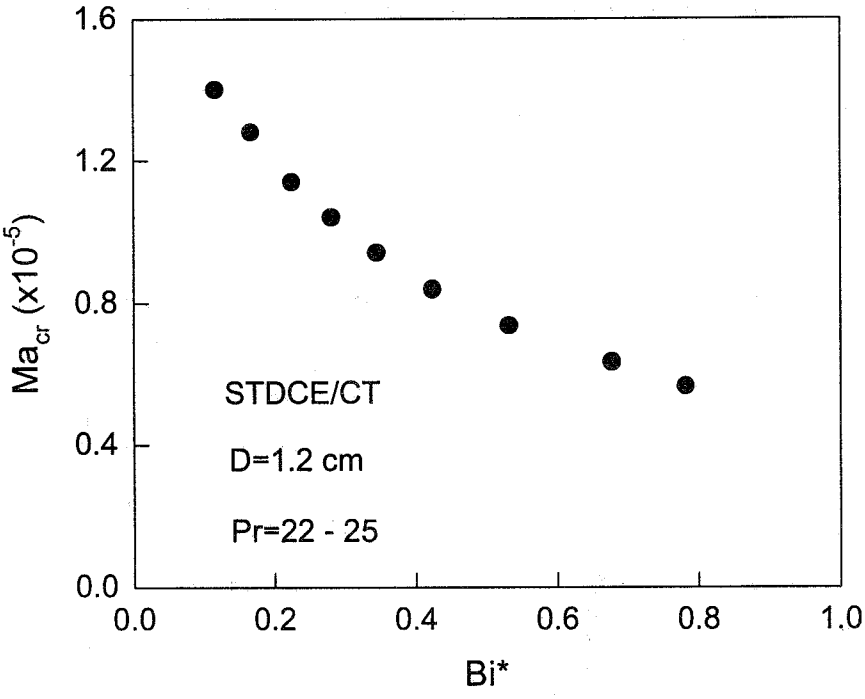


Fig. 20 $Ma_{cr}$ versus Bi* in STDCE/CT configuration

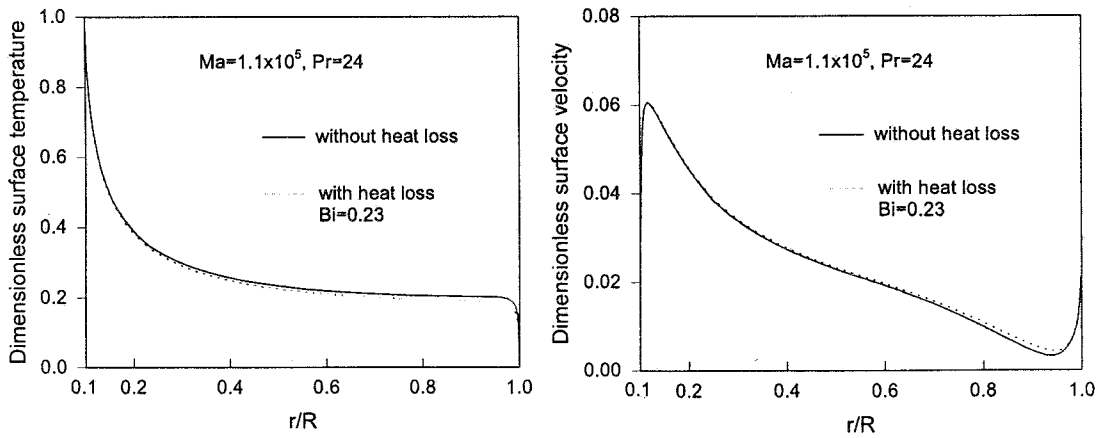


Fig. 21 Surface velocity and temperature distributions with and without heat loss in STDCE/CT configuration

at the onset of oscillations in some situations as discussed earlier. Again, this fact does not seem to be explained by Bi*. (iv) Fig. 19 shows that $Ma_{cr}$ becomes nearly constant when Bi* is large (Fig. 20 also suggests this trend). This implies that the onset of oscillations becomes insensitive to the heat loss as its effect becomes large. This does not seem to make sense.

Although the present heat loss data are based on the numerical simulations, it seems that it is difficult to attribute the present heat loss effect to the basic flow change, based on the above observations. This statement has an important implication. Based on linear stability theory, the transition to oscillatory flow is affected by the surface heat loss through the Biot number, namely, the basic flow field must be altered to change the transition. Therefore, if the present observation is correct, it implies that the oscillation phenomenon is a non-linear process and that the oscillation mechanism is directly affected by the heat loss, even though the basic flow is not much affected. Since the heat loss is generally small, the oscillation process must involve a small but important factor that can be affected significantly by this small heat loss. More work is needed to clarify this important point.

It is interesting to note that the present heat loss effect involving constant $T_H - T_R$ at the onset of oscillations is not observed in concave liquid bridges nor in the CF configuration. All of this information will help us to explain this unique heat loss effect eventually.

## REFERENCES


[1] Preisser, F., Schwabe, D., and Scharmann, A., "Steady and Oscillatory Thermocapillary Convection in Liquid Columns with Free Cylindrical Surface," Journal of Fluid Mechanics, Vol. 126, 1983, pp. 545-567.

[2] Masud, J., Kamotani, Y., and Ostrach, S., "Oscillatory Thermocapillary Flow in Cylindrical Columns of High Prandtl Number Fluids," Journal of Thermophysics and Heat Transfer, Vol. 11, 1997, pp. 105-111.

[3] Kuhlmann, H. C. and Rath, H. J., "Hydrodynamic Instabilities in Cylindrical Thermocapillary Liquid Bridges," Journal of Fluid Mechanics, Vol. 247, 1993, pp. 247-274.

[4] Kamotani, Y., Ostrach, S., and Masud, J., "Microgravity Experiments and Analysis of Oscillatory Thermocapillary Flows in Cylindrical Containers," Journal of Fluid Mechanics, Vol. 410, 2000, pp. 211-233.

[5] Kamotani, Y., Ostrach, S., and Masud, J. "Oscillatory Thermocapillary Flows in Open Cylindrical Containers Induced by $CO_2$ Laser Heating," International Journal of Heat and Mass Transfer, Vol. 42, 1998, pp. 555-564.

[6] Kamotani, Y. and Ostrach, S., "Theoretical Analysis of Thermocapillary Flow in Cylindrical Columns of High Prandtl Number Fluids," Journal of Heat Transfer, Vol. 120, 1998, pp. 758-764.

[7] Pline, A., Zurawski, R., Jacobson, T., Kamotani, Y., and Ostrach, S., "Hardware and Performance Summary of the Surface Tension Driven Convection Experiment-2 aboard the USML-2 Spacelab Mission," Paper IAF-96-J.5.01, presented at the 47th International Astronautical Congress, Beijing, China, 1996.

[8] Patankar, S. V., Numerical Heat Transfer and Fluid Flow, McGraw-Hill, New York, 1980.

[9] Kamotani, Y., Ostrach, S., and Pline, A., "Analysis of Velocity Data Taken in Surface Tension Driven Convection Experiment in Microgravity," Physics of Fluids, Vol. 6,

1994, pp. 3601-3609.
[10] Kamotani, Y., Ostrach, S., and Pline, A., "A Thermocapillary Convection Experiment in Microgravity," Journal of Heat Transfer, Vol. 117, 1995, pp. 611-618.